

Modelling of bubble-mediated gas transfer: Fundamental principles and a laboratory test

D.K. Woolf ^{a,*}, I.S. Leifer ^b, P.D. Nightingale ^{c,i}, T.S. Rhee ^{d,k}, P. Bowyer ^e, G. Caulliez ^f,
G. de Leeuw ^g, S.E. Larsen ^h, M. Liddicoat ^c, J. Baker ^{i,1}, M.O. Andreae ^j

^a Centre for Observation of Air–Sea Interactions and fluxes (CASIX), National Oceanography Centre, Southampton, SO14 3ZH, United Kingdom

^b Marine Science Institute, University of California, Santa Barbara, CA, USA

^c Plymouth Marine Laboratory, Plymouth, United Kingdom

^d Max Planck Institut für Chemie, Atmospheric Chemistry Division, Mainz, Germany

^e Department of Earth and Ocean Sciences, National University of Ireland Galway, Galway, Ireland

^f Laboratoire Interactions Océan–Atmosphère, Institut de Recherche sur les Phénomènes Hors Equilibre (IRPHE-IOA), Marseille, France

^g TNO Physics and Electronics Laboratory, The Hague, The Netherlands

^h Risø National Laboratory, Department of Wind Energy and Atmospheric Physics, Denmark

ⁱ School of Environmental Sciences, University of East Anglia, Norwich, United Kingdom

^j Max Planck Institut für Chemie, Biogeochemistry Division, Mainz, Germany

^k Korea Polar Research Institute, Ansan, South Korea

¹ Meteorological Office, Exeter, United Kingdom

Received 5 October 2005; accepted 13 February 2006

Available online 1 September 2006

Abstract

The air–water exchange of gases can be substantially enhanced by wave breaking and specifically by bubble-mediated transfer. A feature of bubble-mediated transfer is the additional pressure on bubbles resulting from the hydrostatic forces on a submerged bubble and from surface tension and curvature. This peculiarity results in asymmetry of bubble-mediated gas transfer and equilibrium supersaturations of dissolved gases in a bubbly ocean. A second peculiarity is the finite capacity of bubbles, so that the composition of a bubble may change during the exchange. The result is that gas transfer mediated by bubbles is characterized by an altered dependence on the molecular properties of the dissolved gas compared to direct transfer across the main air–water interface. A related phenomenon for bubble plumes with a high void fraction (air volume to total volume ratio) is that the composition of the dissolved gas within the interstitial water of a plume may alter during the exchange process and only mix into the full water reservoir later. Three asymptotes are identified for gas exchange mediated by high-void-fraction bubble plumes and a semi-empirical parameterization of bubble-mediated gas transfer is devised on the basis of these asymptotes, which describes the dependence of the overall transfer velocity on plume properties and molecular properties of the gas.

These models are confronted with data from laboratory experiments. The experiments use artificial aeration with the gas source switched during each run. Measurements of the bubble distribution enable calculation of the theoretical transfer of the gases. A parameterization fits the theoretical transfer satisfactorily. Gas measurements are used to test if the actual transfer of gases is similar to the theoretical transfer. The experimental method enables separation of bubble-mediated transfer from transfer directly across the main air–water interface. The agreement between gas and bubble-derived values of transfer velocity is sufficient to generally validate the theory, but is imprecise. The results suggest that the interstitial water plays a significant role in limiting gas transfer—in particular, limiting transfer of helium—despite the fact that typical void fractions were low (<0.1%). It should be possible to predict

* Corresponding author.

E-mail address: dkw@noc.soton.ac.uk (D.K. Woolf).

gas transfer velocities in the field by simulating oceanic bubble plumes sufficient to constrain that part of the transfer, but targets of 10% or 20% may be beyond reach especially for the most poorly soluble gases (for which the bubble-mediated mechanism is particularly important). These simulations require accurate bubble distributions, void fractions and a good description of the entire plume dynamics. Such simulations are particularly important for interpreting dual tracer and nitrogen/oxygen experiments in stormy conditions, where the relative transfer of different gases is a non-trivial problem.

© 2006 Elsevier B.V. All rights reserved.

1. Introduction

Rates of air–sea gas exchange increase non-linearly with increasing wind speed and sea state (Liss and Merlivat, 1986; Wanninkhof, 1992; Wanninkhof and McGillis, 1999; Nightingale et al., 2000; Woolf, 2005). Part of this increase is likely to be related to breaking waves and the injection of bubbles, but the importance of various mechanisms is still uncertain. Enhancements of gas transfer are expected as a result of the turbulence generated by breaking waves (Kitaigorodskii, 1984; Woolf, 1995), transfer across the surface of bubbles (Merlivat and Memery, 1983; Memery and Merlivat, 1985; Keeling, 1993; Woolf, 1993), and the disruption of the surface microlayer by surfacing and bursting bubbles (Monahan and Spillane, 1984). Similarly, exchange of gases between the atmosphere and inshore- or inland-waters can be by a variety of mechanisms including bubble-mediated transfer (Cirpka et al., 1993). Some attempts have been made to describe the gas transfer due to breaking waves and bubbles (e.g., Asher et al., 1996; Woolf, 1997; Asher and Wanninkhof, 1998), but there are limited data with which to test each model. This paper describes laboratory experiments designed to test and improve these models especially for bubble-mediated transfer. These experiments were a small part of the Luminy project, which is summarised by De Leeuw et al. (2002) and other parts of which are discussed elsewhere (e.g., Leifer et al., 2003; Bowyer and Woolf, 2004; Leifer and de Leeuw, 2006; Leifer et al., 2006; Rhee et al., submitted for publication).

Bubbles offer a second pathway for gases between atmosphere and ocean, in addition to direct diffusion across the main interface. Gas may be injected into the water by first being encapsulated in a bubble and then diffusing across the surface of the bubble. Similarly, gas may evade by diffusing into the bubble and then escaping when the bubble surfaces and bursts. However, this “bubble-mediated” exchange is not the sole pathway of gas transfer and it is difficult to assess the fraction of transfer due to this and other mechanisms (e.g., wind-generated stirring, the turbulence generated by breaking waves and the disruption of the surface by bursting bubbles). In a laboratory setting, some mechanisms can be

excluded or controlled. The laboratory experiments described in this paper allow a detailed analysis of the bubble-mediated transfer of gases.

In the next section, the basic characteristics of bubble-mediated transfer are described and the problem of parameterizing the bubble-mediated transfer is discussed. In Section 3, we summarise the bubble measurements and calculate predicted gas transfer on the basis of the theory described in Section 2. In Section 4, we describe the gas measurements and retrieval of gas transfer velocities. In Section 5, we compare gas transfer velocities inferred from the gas measurements to that expected from the bubble measurements and consider parametric descriptions of the transfer. Finally the findings are discussed and summarised. A list of notation is included at the end of the paper.

2. Characteristics of bubble-mediated transfer

In this section, we consider the basic characteristics of bubble-mediated transfer of weakly soluble gases (we exclude more soluble gases whose “gas-phase resistance” is significant) starting with simple models of the behaviour of a single bubble and then considering parametric descriptions of the behaviour of an arbitrary population of bubbles. Bubble-mediated transfer has been considered by Memery and Merlivat (1985), by Keeling (1993) and by Woolf (1993), while Woolf (1997) proposed a new parametric description. The current work briefly reviews these descriptions but also considers an additional phenomenon: the reduction in total transfer where the plume (consisting of bubbles and their interstitial water) is effectively isolated from the full water reservoir as bubble-mediated transfer proceeds. Since the standard theory applies strictly to trace gases and to gas exchange as opposed to supersaturation effects, we also describe an extension that applies to the exchange of air and a practical estimate of the supersaturation term.

2.1. Single bubble models

A simple model of bubble-mediated air–sea gas exchange considers the independent interaction of each

bubble with the upper ocean. In the case of exchange associated with breaking waves and rain, each bubble evolves as follows: the bubble is formed from air entrained at the sea surface. The bubble exchanges gas with the upper ocean. On surfacing, the bubble bursts and releases its modified contents to the atmosphere. Each bubble is a small intermediate reservoir between the atmosphere and the ocean. The composition of bubbles can change dramatically as a result of exchange with the upper ocean. Instantaneous net transfer of a gas for a submerged spherical bubble of radius, r , is described by:

$$(4\pi r^3/3)dC_b/dt = 4\pi r^2 j(C_1 - C_b\alpha) \quad (1)$$

where j is the “individual bubble transfer velocity”. The dynamics of a bubble depends on compression of the bubble and the flux of the major gases (nitrogen and oxygen), but these effects produce a flux of trace gas unrelated to the surface concentration gradient of that gas and thus contribute to an asymmetry of transfer. Ignoring non-linear effects (caused by changes in bubble size in response to the transfer of air) the resulting effect on the concentration in the full water reservoir can be written as:

$$V_w(dC_w/dt) = A_d\{K_b[(1 + \delta)C_a\alpha - C_w]\} \quad (2)$$

where K_b is the contribution to the transfer velocity between the main air and water reservoirs and depends solely on the partial equilibration of a bubble during its lifetime. Further if we consider a bubble at fixed radius, r and depth z , we find K_b is independent of depth and instead only δ ($=[\rho_w g z + 2\gamma/r]/P_{\text{atm}}$) depends on the additional pressure associated with a submerged bubble.

Thus, if we are interested only in K_b and not δ , it is simplest to ignore the submergence of the bubble and consider only the equilibration with the surrounding water. We can then consider a bubble as a small reservoir volume $V_b = 4\pi r^3/3$ exchanging gas at transfer velocity j across an interface $A_b = 4\pi r^2$ to surrounding water, a reservoir volume V_l . The contribution to the transfer velocity between the main air and water interface can be calculated by summing the exchange of gas across the bubble surface in the lifetime of each bubble and then integrating over all bubbles.

Consider now any arbitrary pair of connected liquid and gas reservoirs, volumes V_l and V_g respectively, each well-mixed but isolated from other reservoirs i.e. a closed system. We can define an “integrated exchange coefficient”, K_{-A} , so that for a gas of Ostwald solubility, α :

$$V_l(dC_l/dt) = -K_{-A}(C_l - C_g\alpha)$$

$$V_g(dC_g/dt) = K_{-A}(C_l - C_g\alpha) \quad (3)$$

If this closed system is initiated at any state (i.e., $C_l = C_{l0}$; $C_g = C_{g0}$), it will always move towards the same final state ($C_l = C_f$; $C_g = C_f/\alpha$), with a common response time, τ . The governing equations can be summarised as follows:

$$C_l = C_f + (C_{l0} - C_f)e^{-t/\tau}$$

$$C_g = C_f/\alpha + [C_{g0} - C_f/\alpha]e^{-t/\tau}$$

$$C_f = (V_l C_{l0} + V_g C_{g0})/(V_l + V_g/\alpha)$$

$$\tau = V_l V_g / [K_{-A}(\alpha V_l + V_g)] \quad (4)$$

The response time, τ , depends on the exchange coefficient, K_{-A} , and the “capacity” of the two reservoirs, V_g/α and V_l . It is useful to consider the response in the limits of either reservoir having a much larger capacity than the other:

$$V_g \gg \alpha V_l \quad \tau \approx V_l / K_{-A}$$

$$V_g \ll \alpha V_l \quad \tau \approx V_g / (K_{-A}\alpha) \quad (5)$$

In the limiting conditions, the sensitivity to the capacity of the larger reservoir is lost, and the response time approaches the residence time of the smaller reservoir. Usually the response time is dependent on the solubility of the gas. This sensitivity is only lost if the capacity of the air reservoir is much higher than the capacity of the liquid reservoir (e.g., very high air volume or very low solubility). We can also estimate the net mass of gas transferred to the water in a time T :

Net transfer

$$= -[1 - \exp(-T/\tau)](C_{l0} - C_{g0}\alpha)V_g V_l / (\alpha V_l + V_g) \quad (6)$$

Again it is the smaller reservoir that mainly limits the total mass transferred. Now if both of these reservoirs are isolated from two much larger reservoirs for only a time T , the resulting transfer between the two large reservoirs depends on this net transfer. This is essentially the basis for modelling bubble-mediated transfer; we consider a bubble as being removed from the main gas reservoir (usually the atmosphere) and exchanging gas with the surrounding water, until it surfaces and “mixes” with the main gas reservoir. Different results follow from assuming it exchanges directly with the entire liquid reservoir (which is effectively infinite) or with the plume water alone, which only later mixes with the main liquid reservoir.

Thus, the simplest model of bubble-mediated transfer (Woolf, 1993; Woolf, 1997) is one in which Eqs. (4)–(6)

are applied to a single bubble, which is the gaseous reservoir, the water reservoir is effectively infinite, and “ $4\pi r^2 j$ ” replaces K_A . As shown by Woolf (1993) the contribution of N bubbles per unit time per unit area each submerged for a time T to the transfer velocity is given by

$$K_b = [N(4\pi r^3/3)/\alpha][1 - \exp(-T/\tau)]$$

$$\tau = r/3j\alpha \quad (7)$$

We might also suppose that a bubble plume may be isolated from the mass of water such that the interstitial water and bulk of water do not mix properly while bubble-water gas exchange is active. This is more difficult to model satisfactorily but a simple approximation is to suppose that each bubble exchanges with a volume V_i of interstitial water, which only mixes with the main water reservoir after the bubble has surfaced. Then we can again apply Eqs. (4)–(6) and a modified version of Eq. (7) follows;

$$K_b = [NX(4\pi r^3/3)/\alpha][1 - \exp(-T/\tau)]$$

$$\tau = Xr/3j\alpha$$

$$X = V_i/[V_i + (4\pi r^3/3)/\alpha] \quad (8)$$

X defines the capacity of the interstitial water to contain a gas as a fraction of the total capacity of the sub-system.

Note that if the capacity of the interstitial water is sufficiently large relative to the capacity of the bubbles, then $X \approx 1$ and the transfer is barely changed. On the other hand, a major reduction in transfer is associated with a relatively small interstitial capacity. For highly insoluble gases, the capacity of the interstitial liquid may be smaller than that of the bubble even for quite small void fractions. We call this restriction of gas transfer in a dense isolated plume “suffocation” since it can be likened to a restriction of healthy breathing (exchange of oxygen and carbon dioxide) in a restricted space. Note that the equations imply that suffocation acts equally on evasion or invasion of gases.

The value of j is determined by the flow around each rising bubble and the properties of the surface of the bubble. Surface-active material can transform the surface of the bubble from being essentially fluid for a “clean” bubble to essentially immobile for a “dirty” bubble. Transfer is more rapid for a clean bubble, and has a different dependence on the molecular coefficient of diffusion, D . Boundary layer theories predict that for a clean bubble, $j \propto D^{1/2}$ and for a dirty bubble, $j \propto D^{2/3}$. The contribution of the bubble to air–water exchange will be independent of solubility and proportional to j if the bubble surfaces before the partial pressure of a gas can change significantly. The contribution of the bubble will be inversely proportional to the solubility of the gas and independent of j if the bubble equilibrates with the surrounding water.

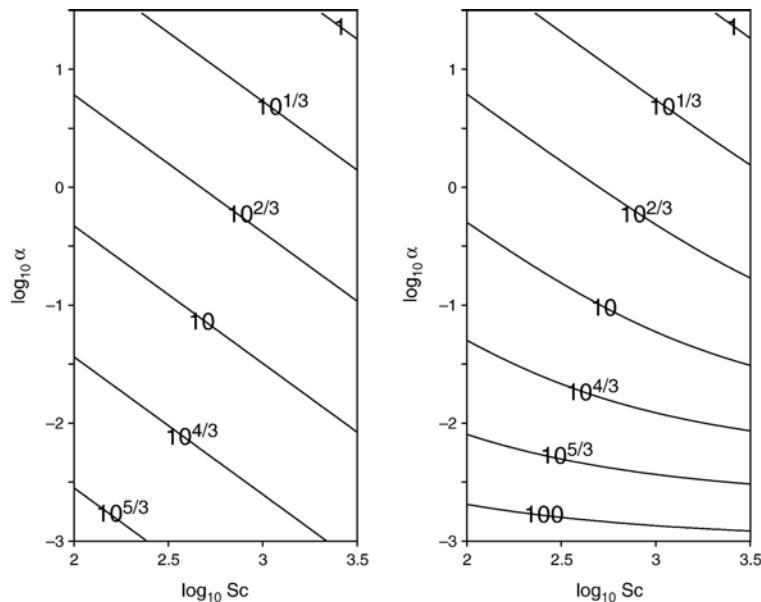


Fig. 1. Parametric descriptions of bubble-mediated transfer velocity. Contours of transfer velocity are logarithmically spaced, 3 contours/decade, units are arbitrary. (a) From Keeling (1993), (b) modified version of “Keeling” as described in the text and Eq. (9).

2.2. Models for bubble populations

The effect of a population of identical (r, j and lifetime) bubbles can be parameterized quite simply, but a real population is not as easy. The basic principles described above imply that the gas transfer velocity attributable to a population of bubbles must increase with increasing values of the molecular diffusion constant D of the gas (or its Schmidt number Sc) and decrease with increasing values of solubility α . Keeling (1993) suggested a power law expression $K_b \sim D^x \alpha^{-y}$ or $K_b \sim Sc^{-x} \alpha^{-y}$ where x and y would be positive constants; Keeling suggested $x=0.35$ and $y=0.3$. A contour plot of the implied variation is shown in Fig. 1a; note that all scales are logarithmic and contour lines are straight and uniformly spaced. As described in the previous subsection, an asymptotic behaviour of bubbles is for gases to equilibrate in small long-lived bubbles. On this basis Asher et al. (1996) proposed an extension of the Keeling model:

$$K_b = a/\alpha + b Sc^{-x} \alpha^{-y} \tag{9}$$

Fig. 1b shows how an arbitrary (but positive) value of “ a ” modifies the Keeling model described in Fig. 1a, increasing the predicted K_b for lower solubilities but leaving values for higher solubilities almost unchanged. While the particular version is arbitrary, it should be noted that the qualitative features of the contour plot are invariant for any positive values of a, b, x and y . (Note

that positive values are demanded by the physical explanation for this parameterization.)

An alternative approach to parameterization was outlined by Woolf (1997). This approach again follows from the behaviour of individual bubbles described earlier in this section but there is a subtle but important difference compared to the origin of Eq. (9). Instead of supposing some bubbles can be characterized by the Keeling model while others are close to the equilibration asymptote, Woolf (1997) proposed that some gases would approximate one asymptotic behaviour in almost all bubbles, while other gases would approach another asymptote. (Since the range in solubility of relevant gases is huge, this appears to be a reasonable proposition if the bubble distribution is not too broad.) Woolf then designed a function with the correct asymptotes and a smooth parametric description of the transition between asymptotes. The argument is summarised here. The following limits must apply:

(full equilibration, e.g., $\alpha \gg 1$)

$$K_b = Q_b/\alpha$$

(no equilibration, e.g., $\alpha \ll 1$)

$$K_b = \int j dA_b / A_d \tag{10}$$

The first limit describes the limit set by the capacity of the bubbles. The second limit describes the individual

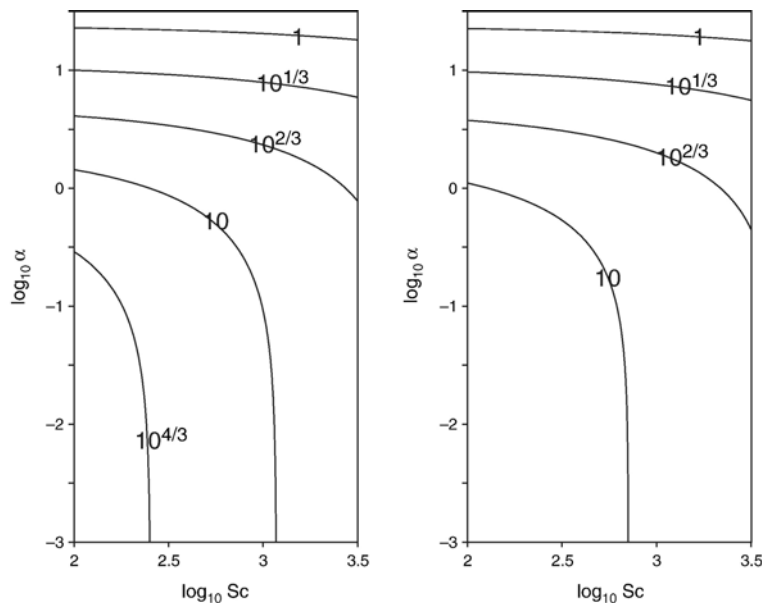


Fig. 2. Parametric descriptions of bubble-mediated transfer velocity. Contours of transfer velocity are logarithmically spaced, 3 contours/decade, units are arbitrary. (a) By Eq. (13) from Woolf (1997), (b) version of Woolf (1997) modified for a void fraction of 25% as described by Eq. (16).

bubble transfer coefficients, j , integrated over all bubble surfaces (per unit area of the main interface). Further simplification is possible where there is a common relationship between j and D for all the bubbles, e.g., if $j \propto D^{1/2}$ then,

$$(\alpha \ll 1) \quad K_b \propto D^{1/2} \quad (11)$$

A parameterization should satisfy the asymptotic behaviour at the two limits and describe the gradual transition between these two limits for a real bubble population. A reasonable form for this parameterization is:

$$K_b = (Q_b/\alpha)[1 + \chi^{1/f}]^{-f}$$

$$\chi = A_d Q_b / (\alpha \int j dA_b) \quad (12)$$

This formula has the correct asymptotes and describes a gradual transition. The non-dimensional parameter, f , is related to the breadth of the bubble distribution. The simple form, $f=1$, performs satisfactorily, but the transition can be modified by setting f to an appropriate value. Woolf (1997) found numerically that the theoretical gas transfer velocity (in cm/h) associated with a shallow flux of clean bubbles at a whitecap coverage of 1% can be described by:

$$K_b = (24.5/\alpha)[1 + \chi^{1/1.2}]^{-1.2}$$

$$\chi = Sc^{0.5}/14\alpha \quad (13)$$

This relationship is plotted in Fig. 2a, using logarithmic scaling and contouring similar to that used in Fig. 1. This model is based on simple equilibration without the suffocation phenomenon described earlier for individual bubbles. If we include the finite volume of interstitial water then the equilibration limit in Eq. (10) is modified to:

$$\text{full equilibration} \quad K_b = Q_p Q_b / (\alpha Q_p + Q_b) \quad (14)$$

where Q_p is the volume flux of the water within bubble plumes (thus void fraction of plumes = $Q_b/[Q_b + Q_p]$). Note that within this one asymptote there are two limiting cases (or two subsidiary asymptotes), one in which gas transfer is limited by the bubble capacity (as in Eq. (10)) and in the other by the capacity of the interstitial water, as follows:

$$\begin{aligned} (\text{full equilibration and } \alpha \gg 1) \quad K_b &= Q_b/\alpha \\ (\text{full equilibration and } \alpha \ll 1) \quad K_b &= Q_p \end{aligned} \quad (15)$$

The “independent bubble model”, Eq. (12), can be modified very simply to a “dense plume model”:

$$K_b = (X Q_b/\alpha)[1 + (X\chi)^{1/f}]^{-f}$$

$$X = \alpha Q_p / (\alpha Q_p + Q_b) \quad (16)$$

The dense plume model can be compared to the independent bubble model in order to highlight the effect of finite void fraction and plume isolation on gas transfer. In Fig. 2b we show results for an identical model to that shown in Fig. 2a, except that a void fraction of 25% is assumed. The results are very similar for soluble gases and the most striking difference is a large reduction in predicted transfer for low solubility, low Schmidt number gases.

We have taken care in presenting 4 generic models of bubble-mediated gas transfer in Figs. 1 and 2) to standardise the presentation. Given this the striking differences between the models, especially between Figs. 1b and 2, are evident and it is clear that not all the models can be appropriate for the same situation. The model described in Fig. 2a is known to fit numerical calculations for a fairly realistic bubble distribution, but has not been validated previously by actual gas measurements; though Cirpka et al. (1993) report satisfactory results for validation of a related model. Asher et al. (1996) were able to fit Eq. (9) to results from a laboratory gas exchange experiment, which on the face of it suggests this model is most practical; but some details are worth reviewing. The sensitivity of the transfer velocity of gases to wave breaking was assumed by Asher et al. to result from both bubble-mediated transfer, K_b , according to Eq. (9) and direct turbulence driven transfer, K_{db} , proportional to whitecap coverage and $Sc^{-1/2}$. For evasion (as reported by Asher and Wanninkhof, 1998), a good fit to the laboratory result scaled to an oceanic whitecap coverage W_c is given by:

$$K_b + K_{db} = W_c \{ [-37/\alpha + 6120 Sc^{-0.18} \alpha^{-0.37}] \quad (17)$$

$$+ (115, 200 - 47 U_{10}) Sc^{-0.5} \}$$

where the term in square brackets clearly derives from Eq. (9) but with a negative “ a ” coefficient. The term that follows is associated with the additional direct transfer resulting from breaking, K_{db} . The bubble-mediated transfer velocity (Fig. 3a) and the total transfer velocity (Fig. 3b) are plotted in a similar style to Figs. 1 and 2 but with the addition of negative-value contours and

symbols indicating the molecular properties of the gases available for the fit (Asher et al., 1996). The consequences of this negative coefficient are evident: a very different functional form to Fig. 1b is seen in Fig. 3a. Given the location of the validation data in the figure, it is clear that the function of the negative “ a ” coefficient is to reduce the sensitivity to solubility in the region of the validation data for poorly soluble gases, but this term also implies physically unsound results (i.e. small or negative transfer velocities) for lower solubilities. Thus, Eq. (17) is successful empirically for the data available, but with a negative “ a ” coefficient it cannot be interpreted physically. For instance, it is difficult to know how the coefficients should change with the bubble distribution.

It is beyond the scope of this paper to reanalyze the results of Asher et al. (1996) fully, but it is worth noting that a combination of the model described by Eq. (16) and a model of the direct turbulent transfer ought to fit successfully to the data. (Given the location of the validation data and the fact that only the total sensitivity needs to be reproduced.) Also, it is explicit how the coefficients of Eq. (16) should be modified for different bubble plume characteristics, so that this is a physical model that might be applied to a variety of environments. Sections 3–5 will investigate if Eq. (13) or Eq. (16) can be successfully applied to the data from the Luminy project.

2.3. Extensions to the model

This final theoretical subsection deals with two outstanding issues that are relevant to analysis and interpretation of data later in the paper. Firstly, we consider the different behaviour of “air” as opposed to a trace gas. Secondly, we evaluate the supersaturation term in Eq. (2) for a simple case.

In general, the bubble-mediated transfer of either a major component of air or “air” as a composite of fairly similar gases (nitrogen, oxygen and argon are quite close in Schmidt number and solubility compared to a broader suite of gases) is complicated by non-linear behaviour since any change in size resulting from air exchange feeds back to the dynamics of the bubble (Woolf and Thorpe, 1991). However, if we can be satisfied that changes in bubble size during the lifetime of the bubbles are negligible (or if bubbles for which this is not true are sufficiently rare), then air exchange is relatively simple. This appears to be the case for the experiments of interest in the Luminy tank (Bowyer and Woolf, 2004) as described in Section 3.1. Therefore, we propose that air can be treated similarly to a trace gas except that the partial pressure of air cannot change so that the “equilibration” phenomenon cannot occur and in the independent bubble model, air transfer will always be controlled by j . However, air transfer can be

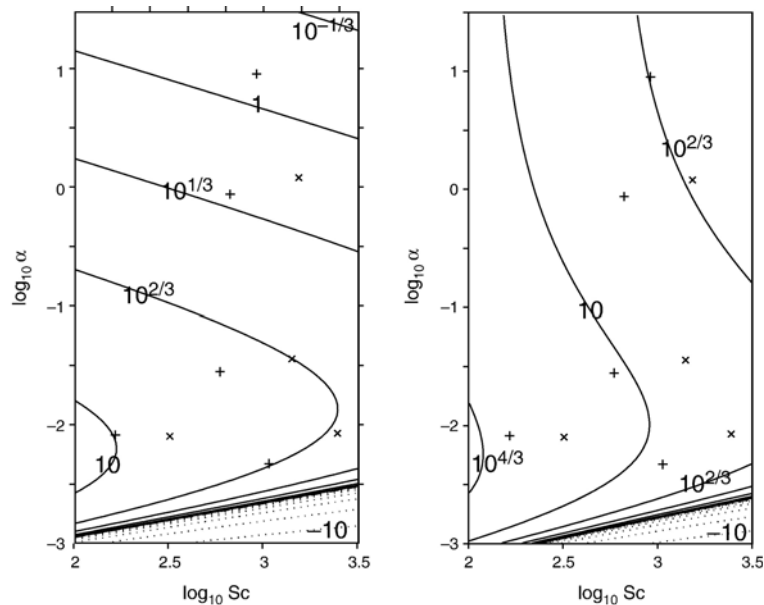


Fig. 3. Parametric descriptions of bubble-mediated transfer velocity. Contours are logarithmically spaced, 3 contours/decade, units are arbitrary. Similarly for negative value contours, but as dotted curves. (a) Bubble-mediated transfer (Asher and Wanninkhof, 1998; Eq. (17)), (b) turbulent and bubble-mediated transfer (Asher and Wanninkhof, 1998; Eq. (17)). Transfer velocity increases towards bottom left, except at very low solubilities where a physically unrealistic decrease in transfer velocity with decreasing solubility is implied. Crosses show the molecular properties of validation data (Asher et al., 1996) for a water temperature of 278 K; plus signs for 293 K.

“suffocated” as in the dense plume model. This assumption is used throughout the analysis of “air data” in this paper, through Eqs. (18) and (19) described below. We predict air transfer from identical bubbles by modifying Eq. (8) to:

$$K_b = NV_i[1 - \exp(-T/\tau)]$$

$$\tau = V_i/4\pi r^2 j \quad (18)$$

and the parametric description given by Eq. (16) is modified to:

$$K_b = Q_p[1 + \chi_a^{1/f}]^{-f}$$

$$\chi_a = Q_p / (\int j dA_b) \quad (19)$$

The equilibrium supersaturation—or asymmetry between evasion and invasion—associated with bubbles rising to the surface has been calculated by Keeling (1993). The asymmetry is less for more soluble gases and small bubbles that will almost equilibrate with water near the surface, since the bubbles will rise only a short distance within the equilibration time. Thus $\delta=0$ will often be an acceptable approximation for fairly soluble gases. On the other hand, in the case of air or a very poorly soluble gas with an equilibration time far greater than the time necessary to surface, equilibrium will occur for bubbles of constant radius and rising at a steady speed when gas evades from the bubble in the lower half of its trajectory and invades nearer the surface, which implies $\delta \approx$ average hydrostatic pressure/atmospheric pressure $\approx \rho_w g z / 2P_{\text{atm}}$ for bubbles rising from depth z ; e.g. $\delta \approx 3\%$ for $z=0.6$ m. Observed equilibrium supersaturations of air in these experiments were typically between 3% and 4% (Bowyer and Woolf, 2004); these slightly elevated values might be related to higher exchange early in the rise when the bubbles are cleaner. Note that the deduced equilibrium supersaturations are assumed in the analysis described in Section 4.2 and results are slightly sensitive to these assumed values.

3. Bubble Experiments

3.1. Bubble measurements

The main “Luminy” experiments were conducted in the 40-m-long air–sea interaction simulation tunnel at the Institut de Recherche sur les Phénomènes Hors Equilibre, Laboratoire Interactions Océan-Atmosphère de Luminy (IRPHE-IOA) in Marseilles, France, in March 1997. The tank was filled with 95 m³ of municipal fresh water, which

was replaced weekly. The tank slopes slightly so that the depth of water varies along its length, averaging ~ 0.9 m. Bubble plumes were produced by aeration devices, large arrays of porous ceramic tubes, that were submerged to ~ 0.6 m depth in the water from near the upstream edge of the tank to 30 m fetch. A wide variety of experiments were conducted in the tunnel involving various combinations of artificial wind and waves in addition to manipulations of the aeration (De Leeuw et al., 2002); here we focus solely on experiments at low wind where the aerators were the sole source of bubbles. The supply of air to the aerators was monitored, giving an accurate measurement of the total aeration rate. Measurement of the distribution of bubbles constituting this total flow was more difficult. The optical methods used to measure the bubble distributions and the results for the aerators are described in detail by Leifer et al. (2003). Below, we will briefly review these results and discuss implications for the gas flux.

The bubble concentrations from the aerators were calculated from a scan on March 13, 1997 along the length of the tunnel and were reported by Leifer et al. (2003; Fig. 6). Concentrations vary greatly in the heterogeneous field associated with the bubblers, but the quoted distribution is an average valid for 60 m² of the tunnel. The total bubble population can be subdivided into 3 main sub-populations: sub-100 μm radius bubbles possibly associated with a bubble-bursting mechanism (Leifer et al., 2000), a narrow and prominent distribution peaking at ≈ 275 μm radius and a broad tail of bubbles > 700 μm . The first sub-population is relatively difficult to model properly, but (as discussed below) is unlikely to be significant to gas exchange. The central sub-population is accurately constrained by the measurements. Most of the aerators produce bubbles primarily in the central sub-population while a few “faulty” aerators primarily produce larger bubbles. The large bubbles are relatively rare and emanate from a few point sources so that the main problem is sampling this sub-population sufficiently so that the concentration is accurate. The measurement techniques have been demonstrated for bubbles up to 5 mm in radius, and observations show that bubbles in excess of 2 mm are rare from the aerators but the actual distribution is uncertain due to poor sampling. In Fig. 4a we show the bubble size distributions on a semi-logarithmic scale. The curve is a fit to the observations except the concentration of large bubbles was reduced from a first guess consistent with the faulty aerators being over-represented in the scan and to ensure that the calculated volume flux is equal to the measured supply to the aerators (see later). (Note that while the frits in total were numerous and randomly distributed by design, there were very few faulty frits and the scan may by chance

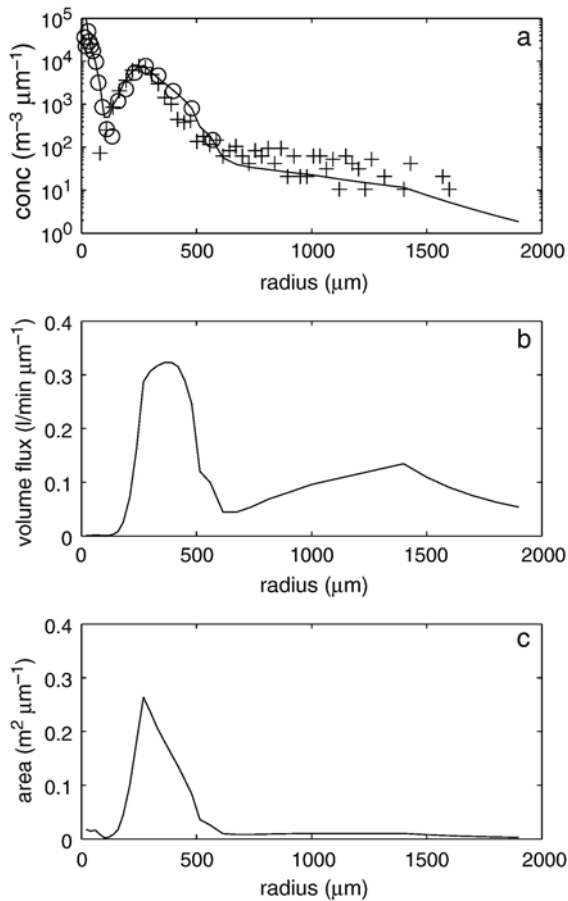


Fig. 4. Bubble size distribution from the aerators (based on measurements reported by Leifer et al., 2003). (a) Semi-logarithmic plot of bubble concentration versus bubble radius; curve is a smooth fit used in numerical calculations, symbols are original observations. (b) Volume flux of bubbles versus radius. (c) Surface area of bubbles versus radius.

have over-represented these.) We have assumed an r^{-2} distribution for bubbles between 1 mm and 1.5 mm radius; r^{-6} for 1.5 mm to 2 mm.

Modelling air–water gas transfer rates also requires the trajectory of the bubbles to be defined. All of the larger ($r > 100 \mu\text{m}$) bubbles should rise at their terminal velocity from 0.6 m depth to the surface with only a few percent change in radius (due to expansion under lowering pressure and as a result of air exchange). For simplicity, the more substantial size change of very small bubbles is neglected. Though the bubbles are rising at terminal velocity they are also carried in a flow associated with the rising bubble plumes. This secondary flow ensured that even the smallest bubbles reliably surfaced within ~ 15 s. Observations suggest that the total upward velocity can be approximated by: rise velocity (m/s) = $0.04 + 0.3r$, where r

is the radius in millimetres; up to a maximum of 0.28 m/s for large bubbles.

As described in Section 2, both the available surface area and the volume flux of bubbles are highly significant to the theoretical gas transfer velocities. The total volume flux is constrained by the flow meter measurement, ≈ 209 l/min. The surface area is simply calculated from the distribution of bubbles. Volume flux and surface area distributions are plotted in Fig. 4b and c; note that we use a linear plot since then the relative area under each graph in each size range is a direct indicator of the importance of that size range to gas transfer. The very small bubbles while numerous are revealed to be unimportant to air–water gas transfer rates, while the other two sub-populations are both highly significant. Approximately 90 l/min of the total 209 l/min is contained within bubbles less than 585 μm radius while 55 m^2 of a total 66 m^2 of surface area are contained within these bubbles. Thus, the larger bubbles may be slightly more important than the smaller bubbles for more soluble gases, but the smaller bubbles should be more important for very poorly soluble gases.

3.2. Forward model of gas transfer velocities

The description of the bubble distribution in the previous subsection is sufficient to apply the theory described in Section 2, in order to estimate the gas transfer

Table 1
Various estimates of bubble-mediated transfer velocity

Type of estimate	Gas					Mean bias	rmse
	SF ₆	He	CH ₃ Br	N ₂ O	Air		
<i>March 13</i>							
Gas	46	58	2.75	3.5	85		
Bubble, clean	69.4	159.5	2.6	15.8	97	29.8	47.2
Bubble, dirty	17.6	57.1	2.4	9.8	27	-16.3	29.0
Bubble, mixed	28.7	81.9	2.6	14.8	41.5	-5.15	24.0
Fit 1	58.6	66.7	2.5	14.3	64.9	2.35	12.3
Fit 2	59.4	66.3	2.5	14.2	64.8	2.39	12.4
<i>March 20</i>							
Gas	36	60	2.0	5.5	46		
Bubble, clean	41.9	96.3	1.6	9.5	58.6	11.7	17.5
Bubble, dirty	10.6	34.4	1.4	5.9	16.3	-16.2	20.9
Bubble, mixed	17.3	49.5	1.6	8.9	25.1	-9.4	13.5
Fit 1	35.6	60.1	1.5	9.3	46.0	0.6	1.7
Fit 2	36.1	60.2	1.5	9.0	45.8	0.62	1.61

Other estimates are compared to those derived from actual gas measurements, including an overall misfit: mean bias and mean root mean square error (rmse). All values are given in centimetres/hour (1 cm/h = 3.6×10^{-5} m/s). For each date, the second group of results is calculated according to the individual bubble model. A third group describes two fits of the dense plume model.

velocities associated with these bubble populations. We do also need to define hydrodynamic parameters of the bubbles especially the individual bubble transfer velocity, j . These parameters were reviewed within the Luminy project (Patro et al., 2002; Leifer and Patro, 2002). A critical matter is whether the bubbles behave as “clean/mobile” or “dirty/immobile”. This is particularly important for millimetre-scale bubbles for which mobile bubbles have a greatly enhanced j . Most sources suggest that while natural systems are never truly “clean”, very large bubbles generally behave as if they have “mobilized” surfaces with a transition from immobile to mobile at 500–700 μm radius. Here, we calculate gas transfer velocities assuming “dirty” or “clean” formulae using the simplifications and formulae described by Woolf (1993). (Note also the special treatment of air as described in Section 2.) We subdivide the population into small (<585 μm), and large (>585 μm) and consider 3 cases: all bubbles clean, all bubbles dirty and only bubbles <585 μm dirty (denoted “mixed” hereafter). Results for five key gases are described in Table 1.

The preceding results depend on the assumption that the water surrounding the bubbles is well-mixed with all the water in the tank. As discussed in Section 2, gas transfer may be “suffocated” if the water immediately surrounding bubbles is effectively isolated from the main bulk of the water. The void fraction can be calculated from the mean bubble distribution and is only 0.03%. Many bubbles are congregated in relatively dense streams emanating from each device, but these diverge as the bubbles surface. Estimates for two plumes 0.07 m below the surface (Fig. 5 of Leifer et al., 2003) are 0.03% for a regular device and 0.15% for the larger bubbles from a broken device. The “typical” void fraction experienced by the bubbles is difficult to estimate from the bubble measurements, but should from these observations be fairly low. However, we repeat the modelling described in the previous paragraph with the modification of a finite void fraction. We assume a range of void fractions (identical for every bubble size), which is the fraction of the bubble+surrounding water volume occupied by the bubble, and calculate gas transfer velocities. Results for a few illustrative gases for the case of mixed clean and dirty bubbles are shown in Fig. 5. For highly soluble gases the limited interstitial water volume is never significant, but for lower solubility gases dramatic reductions in gas transfer are expected for void fractions of only a few percent (Fig. 5a). Another important feature is the much greater effect of “suffocation” on gases with high molecular diffusion coefficients. This is illustrated in Fig. 5b where the ratio of helium-4 and SF_6 transfer velocities reduces from around 2.5 for no

suffocation to just over 1 for high void fractions. Note that the ratio for direct transfer is also ≈ 2.5 so that this low ratio is an exceptional feature.

These numerical models are sufficiently simple to run for many thousands of gas properties and allow us to explore the relationship of transfer velocity to gas properties in detail. In Figs. 6 and 7 (full curves) we present contour plots of direct calculations for permutations of diffusion coefficient and Ostwald solubility for the bubble distributions and formulae described above. Fig. 6 shows results for “mixed” clean and dirty bubbles, while Fig. 7 shows results for clean bubbles. Results are presented for zero void fraction (Figs. 6a and 7a) and for

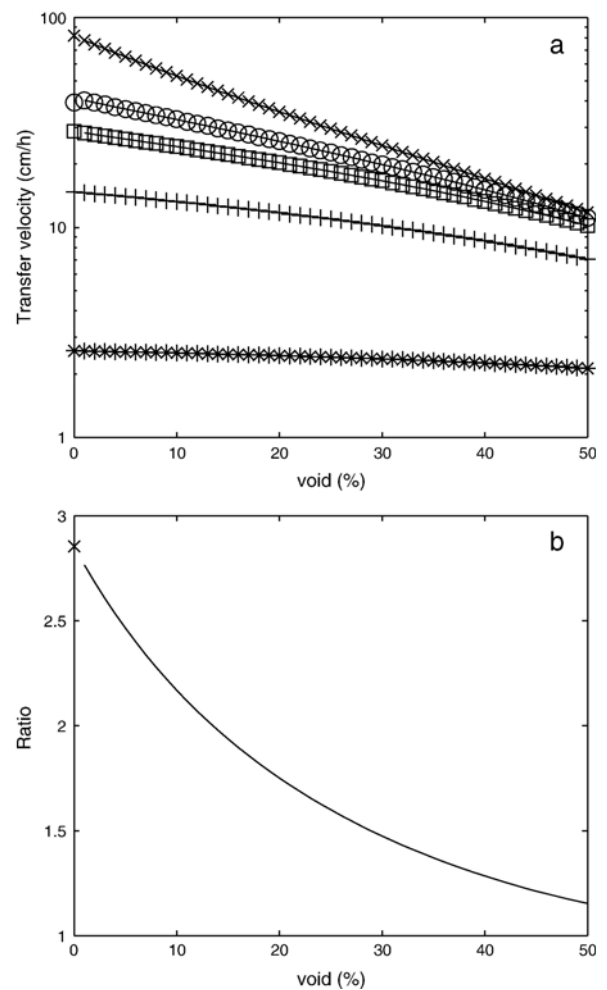


Fig. 5. The effect of void fraction on gas transfer. Values are calculated from the bubble distribution assuming small bubbles are dirty and large bubbles are clean as described in the text. (a) Bubble-mediated transfer velocity versus void fraction for helium-4 (cross), air (circle), sulphur hexafluoride (square), nitrous oxide (plus) and methyl bromide (asterisk). (b) Ratio of transfer velocity of helium to that of sulphur hexafluoride.

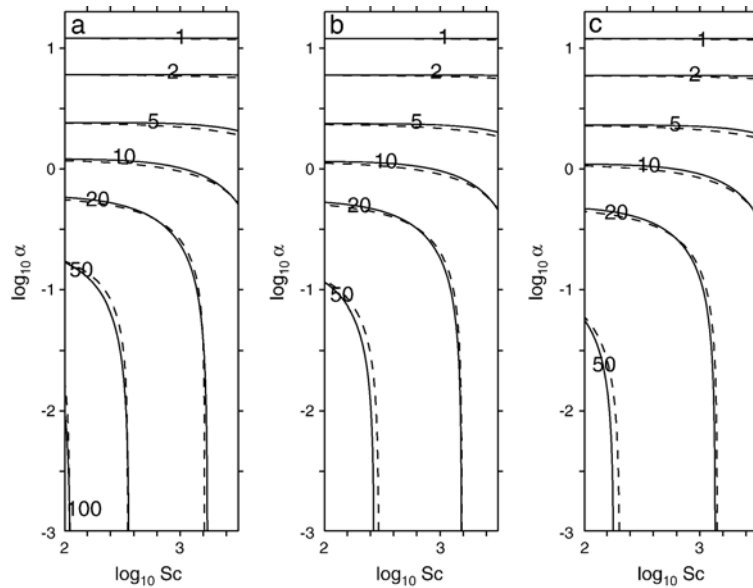


Fig. 6. Contour plots of bubble-mediated transfer velocity on a logarithmic plot of Ostwald solubility (0.001 to 10) versus Schmidt number (100 to 3000). Values are calculated from the bubble distribution assuming small bubbles are dirty and large bubbles are clean (mixed case). Contours in cm/h as labelled and approximately logarithmically spaced; full curves are from direct calculations and dashed curves are a parametric fit from Eqs. (12) and (16) ($n=0.6$, $\lambda=Sc^n/(\chi\alpha)=140$, $f=0.75$). (a) No suffocation (void fraction=0); (b) void fraction=5%; (c) void fraction=10%.

void fractions of 5% (Figs. 6b and 7b) and 10% (Figs. 6c and 7c). Note that the void fraction is progressively more influential for lower Schmidt numbers and lower solubilities. Note also that the contours strongly suggest

parameterizations described by Eq. (12) or (16) are appropriate, while other options discussed in Section 2 can be ruled out. In Fig. 6 we include, as dashed curves, contours given by fitting these equations; note that two

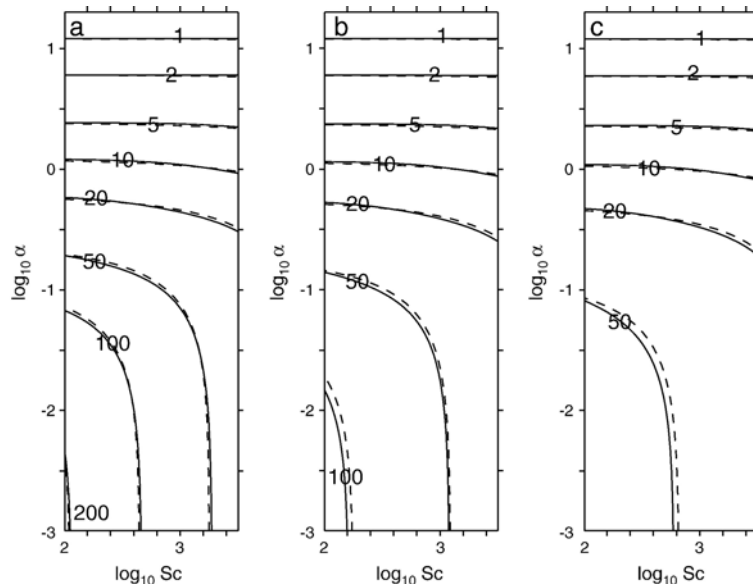


Fig. 7. Contour plots of bubble-mediated transfer velocity on a logarithmic plot of Ostwald solubility (0.001 to 10) versus Schmidt number (100 to 3000). Values are calculated from the bubble distribution assuming all bubbles are clean. Contours in cm/h as labelled and approximately logarithmically spaced; full curves are from direct calculations and dashed curves are a parametric fit from Eqs. (12) and (16) ($n=0.5$, $\lambda=Sc^n/(\chi\alpha)=175$, $f=0.9$). (a) No suffocation (void fraction=0); (b) void fraction=5%; (c) void fraction=10%.

parameters, volume flux and void fraction, are pre-determined while “ χ ”, “ f ” and (within tight restraints) “ n ” can be adjusted. Single values of these parameters are sufficient to produce a good simulation of the direct results for all void fractions; as shown by the near coincidence of the two sets of contours. This is repeated in Fig. 7, where in this case $n=1/2$ by construction.

The values of the non-dimensional parameters “ χ ” and “ f ” differ from those suggested by Woolf (1997; Eq. (13) in this paper). “ f ” is slightly smaller for the bubble distribution here due to the narrower distribution. “ χ ” is substantially larger here as the bubbles are generally smaller and also rise from a greater depth.

4. Measurement of gases

4.1. Gases and techniques

We measured up to eight gas transfer rates: nitrous oxide (N₂O); dimethyl sulphide (DMS); methane (CH₄); carbon dioxide (CO₂); helium (He); sulphur hexafluoride (SF₆); methyl bromide (CH₃Br); and total air. These gases, except for He, have significant environmental impact. They also cover a broad range of physicochemical properties, which allows us to explore the nature of their effect upon transfer velocities. However, satisfactory results for carbon dioxide, dimethyl sulphide and methane are not available for the experiments discussed here. Sources of the physicochemical parameters and more of the measurements are described by Rhee et al. (submitted for publication).

The method of separating bubble-mediated transfer and direct transfer requires high concentrations in the headspace of the tank, which favours invasion experiments (net gas transfer from headspace to water). These experiments were performed after injecting pure gases into the headspace to make the gas concentrations in the headspace greater than those in the water. Unfortunately the headspace of the tank was very leaky, so that most of this gas leaked out into the laboratory rather than being transferred to the water, which shortened the period when there was a substantial air–water concentration difference. In one of the experiments described here, a second addition of gases was made to the headspace.

In the experiments described here, gas exchange as a result of artificial aeration was of primary interest but wind and (in one experiment) paddle-generated waves were used to produce fairly realistic surface roughness; the wind also ensures that the headspace remains well-mixed. The experiments described here were conducted at a reference wind speed of 2.5 m/s and can be compared to experiments without the aeration devices. A current and

the recirculation system in the tank ensures that the water volume is reasonably well-mixed, which can also be monitored through the total gas measurements (Bowyer and Woolf, 2004). The water always circulated at 5 cm/s in the same direction as the wind. Waves could be generated by a paddle at the upwind end of the tank. Wind speed and water current were generated by means of an axial fan and a helicoidal pump respectively, which were installed at the return air-duct and aqueduct.

The aeration devices could be supplied from either the headspace air or air from outside the laboratory. The flow rate could be adjusted and also the aeration devices were separated into sets (each randomly distributed over 60 m²) and the supply could be directed to one or more sets.

Three different methods were employed to sample the dissolved gases: continuous equilibration using a shower-type equilibrator (N₂O) (Weiss et al., 1992); a purge-and-trap method (SF₆, CH₃Br); and static equilibration using a syringe (He). All gas concentrations in the headspace and water, except total air, were determined using gas chromatographic systems.

N₂O was separated using a packed column, Spherocarb™ (Phase Separations, Inc.), at a constant oven temperature of 85 °C or 90 °C. N₂O was detected by an electron capture detector (ECD) at 300 °C. The uncertainty for analyses was estimated to be 2%.

The separation of He was achieved using a column (1/8 in. × 4 m) packed with molecular sieve 5A (mesh 80/100) at 30 °C and it was detected by a thermal conductivity detector (TCD) at 100 °C (Upstill-Goddard et al., 1991). The estimated analytical errors for the headspace gas and dissolved gas were 2% and 5%, respectively.

SF₆ was trapped on Porapak QS in liquid propanol at –60 °C, thermally released to a gas chromatograph, and detected by ECD (Law et al., 1994). Headspace and dissolved gases were analyzed with an uncertainty of 1% and 5%, respectively.

CH₃Br was cryogenically focused on a 1/16 in. stainless steel trap at –150 °C, thermally desorbed at 100 °C, separated by a PoraPLOT Q capillary column (0.53 mm ID × 50 m), and then detected by ECD. N₂ was used as the make-up gas (30 ml/min) (Krysell and Nightingale, 1994). The analytical uncertainties were estimated as 2% for the sample from the headspace and 5% for the dissolved gas.

Total dissolved air was measured using a very thin silicone membrane tube. As dissolved gas permeates and then equilibrates through the silicone membrane, the pressure inside the silicone membrane tube represents the sum of the partial pressures of all the dissolved gases. The pressure inside the silicone membrane tube was measured with a piezoresistive differential pressure

sensor. The response time of the instrument was less than 20 s. The pressure was measured relative to the hydrostatic pressure at the measuring location. Further details are described by Bowyer and Woolf (2004).

A Pitot-tube and hot X-wire anemometers were employed to measure the mean wind velocity and the instantaneous velocity of air flow near the air–water interface in the longitudinal and vertical directions at different heights. The inertial-dissipation method was applied to determine the vertical turbulent momentum flux, which is directly related to the friction velocity of the wind at the water surface. The anemometer was installed on a carriage that moved back and forth from 14 m to 30 m fetch downstream in the tank, so that values of friction velocity were determined at several fetches covering 40% of the full fetch. To characterize wave field, two capacitance wave gauges were mounted on the carriage beside the anemometer.

Two sets of experiments are reported here. In both cases, the aeration devices were first supplied from air outside the laboratory (determined to contain negligible concentrations of sulphur hexafluoride, helium, nitrous oxide and methyl bromide) and then the supply was switched quickly to the headspace of the tank (high in all these gases). In the first case, the action of the bubble-mediated transfer is to strip these gases from the water, while transfer across the main air–water interface of the tank will be directed into the water; thus concentrations will tend towards a balance between the stripping and direct transfer. When the supply is switched to the headspace, the bubble-mediated transfer will be into the water and a more typical invasion experiment results.

The first pair of experiments was conducted on March 13 (and included the bubble measurements reported in Section 3). Throughout the experiment, air was supplied at a rate of 209 l/min to two sets of aerators. The paddle was operated at 1.5 Hz to generate waves. A friction velocity of 0.09 m/s was estimated for the reference wind speed of 2.5 m/s. The water warmed slightly during the day as a result of the operation of the water pump but averaged 21.5 °C. The second pair of experiments was conducted on March 20. Throughout air was supplied at a rate of 126.2 l/min to a single set of aerators. The paddle was not used and a friction velocity of 0.07 m/s was estimated for the reference wind speed of 2.5 m/s. The average water temperature was 21.8 °C.

4.2. Gas measurements and retrieval of transfer velocities

The gas measurements (excluding air) for March 13 are reported in Fig. 8 and for March 20 are reported in

Fig. 9. The change in supply has an obvious effect on the time series of concentrations in water of these gases and the time series are used to separate bubble-mediated and direct transfer as described below. In the case of total gas transfer, the manipulation of the supply has no effect and only a single value of the total transfer velocity of air can be estimated (95 cm/h for March 13 and 54 cm/h for March 20 as reported by Bowyer and Woolf, 2004).

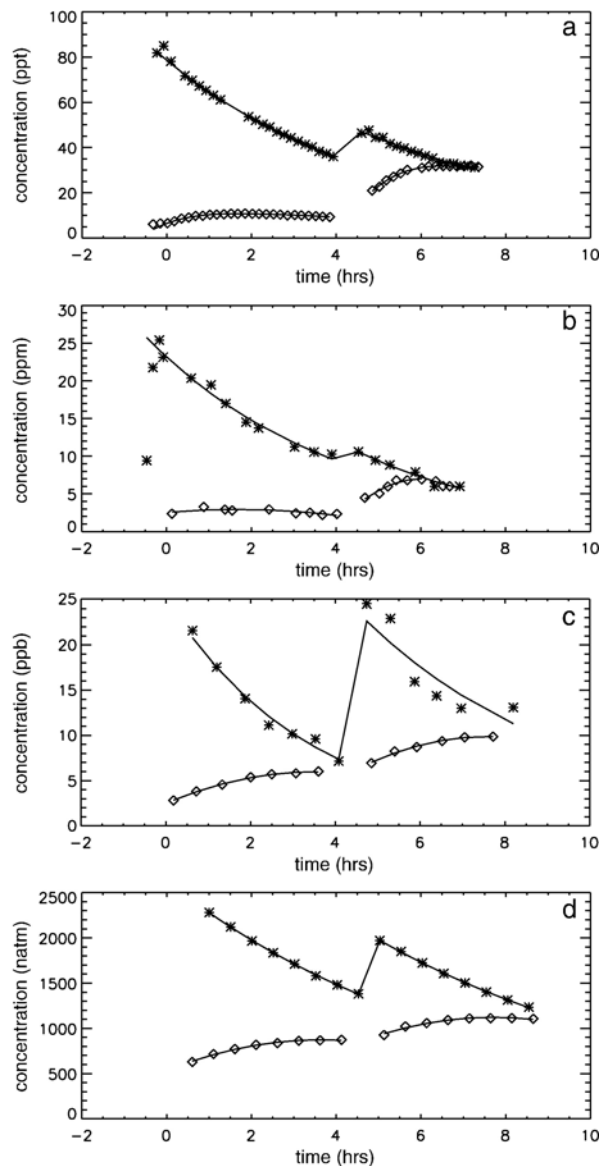


Fig. 8. Time series of concentrations during experiments on March 13. Measurements of water concentration are shown by diamonds, $C_a\alpha$ by asterisks. Fits of the time series are shown by curves. Four gases are shown, (a) SF_6 , (b) He, (c) CH_3Br and (d) N_2O . All concentrations in linear units.

For most experiments, including all experiments *without* the aeration devices and experiments *with* the aeration devices where these devices were fed from the headspace, the budget for the dissolved gas in the tank can be written as:

$$V_w(dC_w/dt) = -K_T A_d [C_w - \alpha C_a (1 + \Delta)] + \Sigma_w \quad (20)$$

or,

$$V_w dC_w/dt = A_d \{ K_b [(1 + \delta) \alpha C_a - C_w] + K_d [\alpha C_a - C_w] \} + \Sigma_w$$

When the aerators were fed from outside the laboratory, an alternative equation results:

$$V_w dC_w/dt = A_d \{ K_b [(1 + \delta) \alpha C_{atm} - C_w] + K_d [\alpha C_a - C_w] \} + \Sigma_w \quad (21)$$

Σ_w represents the production or consumption of the gases in the tank by microbial activities or chemical reaction. He and SF₆ are inert, but this term must be evaluated for the other gases. Respiration (consumption of oxygen; Bowyer and Woolf, 2004) and degradation of methyl bromide (Rhee et al., submitted for publication) were both detected but in the context of these experiments were considered negligible. For nitrous oxide, no production or consumption was detected in control experiments.

The supersaturation term, Δ , is generally fairly small and predictable (see Section 2.3). Since every “unknown” in the equations increases the uncertainty of the remaining unknowns, we tended to assert a value for Σ_w ($=0$) and Δ ($=0$ in most cases, but 3% for SF₆ and He in the aeration experiments) in favour of reducing uncertainties in the transfer velocities. These assumed values of Δ are uncertain to $\sim 1\%$, this level of uncertainty does not add significantly to the true uncertainty in the transfer velocities.

The basis of the separation between bubble-mediated exchange, K_b , and direct exchange, K_d , is that if C_{atm} and C_a are quite different it should be possible to determine both components of transfer from a time series following Eq. (21). For the trace gases, the atmospheric concentration is negligible ($C_{atm} \ll C_a$, $C_{atm}/H \ll C_w$) and where the aerators were fed from outside air, the mass budget simplifies to,

$$V_w dC_w/dt = A_d \{ -K_b C_w + K_d [C_a \alpha - C_w] \} \quad (22)$$

In this situation, the exchange of gases across the surface of the bubbles has a solely “stripping” effect. In an

invasion experiment, the stripping of the water by the bubbles competes with invasion across the main surface of the tank, and C_w will plateau long before it approaches $C_a \alpha$. This can be seen in the first half of the time series in Figs. 8 and 9. In principle, these segments are sufficient to estimate both components of transfer. However, while these segments accurately describe the ratio of the two components—determined by the

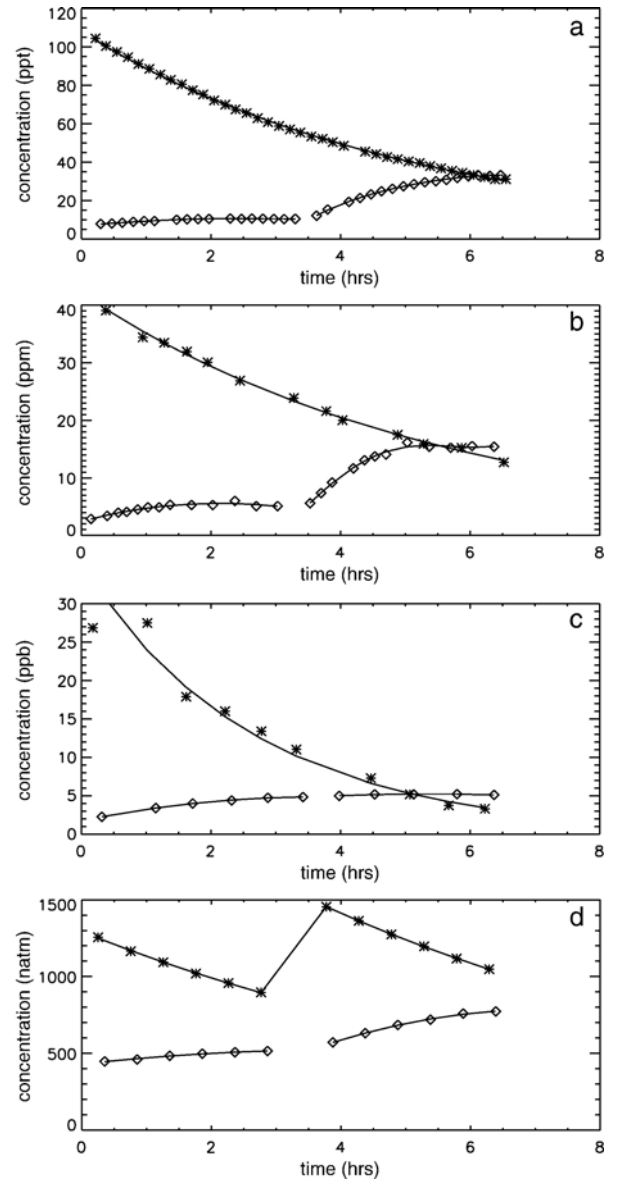


Fig. 9. Time series of concentrations during experiments on March 20. Measurements of water concentration are shown by diamonds, $C_a \alpha$ by asterisks. Fits of the time series are shown by curves. Four gases are shown, (a) SF₆, (b) He, (c) CH₃Br and (d) N₂O. All concentrations in linear units.

“balance point”—their absolute magnitude is difficult to fix adequately from these segments. However, an ordinary invasion experiment is suitable for estimating the total transfer velocity as in the second half of each experiment that follows Eq. (20), and thus both segments of the time series are useful.

In each experiment, the task is to estimate the “unknowns” given time series measurements of C_a , C_w and temperature (from which the instantaneous solubility can be calculated). A number of slightly different (curve-fitting and interpolation) methods can be used to estimate C_a , and dC_w/dt at instances when C_w was measured. We can then estimate K_T on a criterion of “maximum likelihood”. A number of slight variations on this method have been tried, but the results reported here are reached as follows. A fit to the time series in C_w and C_a is estimated (a polynomial to each segment of C_w and an exponential fit to C_a ; these are the curves in Figs. 8 and 9). These fits determine C_a and dC_w/dt at any time including the measurement times of C_w . We can then apply Eq. (20) or (21) as appropriate to calculate a second value of dC_w/dt given a guess of the transfer velocities at each of the measurement times. The “best” set of transfer velocities are those that minimise the sum of the square of differences between paired values of dC_w/dt , summed over the experiment.

Measurement errors in C_w (leading to magnified errors in dC_w/dt) are usually the limiting factor in the accuracy of estimates of the transfer velocities. Confidence limits can be placed using a variant of “the bootstrap method” (Press et al., 1992). In this method, simulated data sets are created by selecting at random n sets of values $[t_i, C_{w,i}]$ from the original n measurement pairs *with replacement*. These synthetic time series are analyzed identically to the original time series and a large number of estimates of the transfer velocities are accumulated. The distribution of estimates from a large number of simulations forms the basis of confidence limits on the original estimate. The effect of measurement errors in other variables could be tested similarly, but the confidence limits reported below are 90% limits for errors in C_w only.

The time series for all the trace gases reported here are shown in Figs. 8 and 9. It is apparent that some of the measurements probably fall outside the nominal analysis accuracy reported in Section 4.1, thus motivating smoothing by the fits (shown as curves). The analysis is illustrated by results for helium on March 13, as shown in Fig. 10. Fig. 10a shows a contour plot of the sum of square errors for various guesses for the first half of the experiment only. Fig. 10b shows values of transfer velocity from the bootstrap procedure described above, again for only the first half of the experiment. These

results illustrate that the balance between the two components of transfer velocity is fixed with reasonable precision by the first half of the experiment (that is “permissible values” fall along a straight line of almost constant $K_a:K_b$), but the absolute value of each is highly uncertain. Generally, this deficit can be filled by the second half of the experiment. However, in this case the “invasion experiment” is quite short and conducted at a fairly small concentration difference. Thus, as seen in Fig. 10c and d, in this case the complete experiment narrows confidence limits substantially but leaves a large uncertainty. Note also that these confidence limits exclude bias resulting from systematic errors. Where the concentration difference is small, fairly minor systematic error in C_a or C_w will result in a major bias in K_T . Thus the accuracy of measurements and the precise conduct of the experiment have major consequences for the accuracy of the results. Much better results were achieved on March 20 by a few improvements in experimental procedure. In particular, generally higher concentration differences for the second half of the experiment contributed to narrower confidence limits.

Results for the total transfer velocity and its two components, including confidence limits are shown in Table 2.

5. Comparison

Estimates of the transfer velocity of four gases in two separate experiments have been described in Section 4 and are summarised in Table 2. The estimates for bubble-mediated transfer are included in Table 1, where they are compared to various sets of results for the same gases following from the calculations described in Section 3. Estimates of the total transfer velocity of air on the same 2 days have been made by Bowyer and Woolf (2004) and we subtract a rough estimate of the direct transfer (10 cm/h for March 13 and 8 cm/h for March 20) to give an estimate of the bubble-mediated transfer velocity, which is also included in Table 1. We have noted a number of substantial uncertainties in Sections 3 and 4, which should be remembered before interpreting the comparison.

As described in Section 3, estimates from the bubble distribution can be made for a number of hydrodynamic conditions and for different void fractions. Further a shortcut to any of the solutions can be made through a parametric equation that quite precisely fits the full calculation. One group of results in Table 1 is calculated from the individual bubble model and for three hydrodynamic conditions for each experiment. The bubble measurements were made on March 13 and the

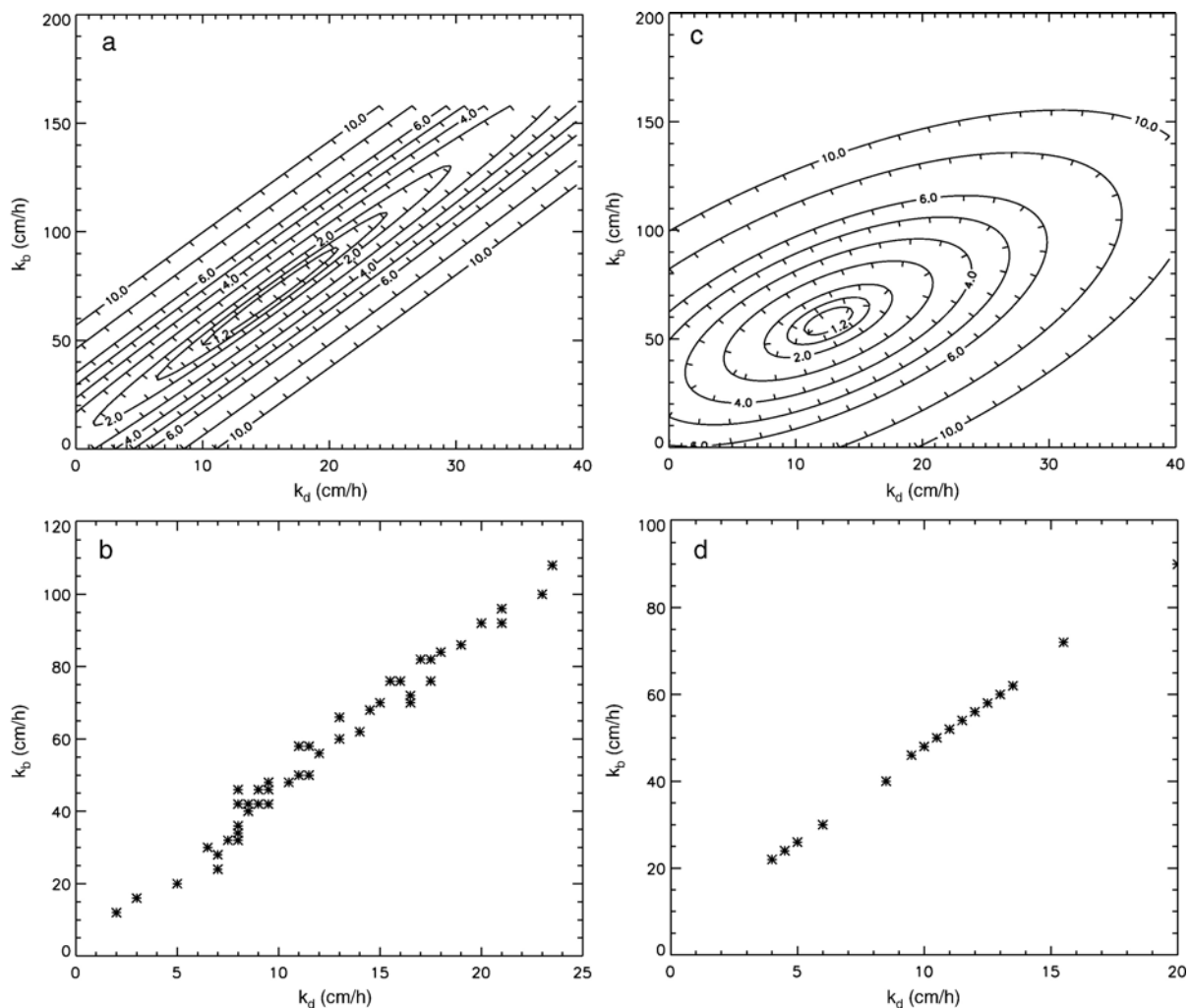


Fig. 10. Minimisation of errors for He on March 13. (a) Contour plot of errors for first half of the experiment. (b) Scatter plot of values from bootstrap procedure for the first half of the experiment. (c) Contour plot of errors for full experiment. (d) Scatter plot of values from bootstrap procedure for full experiment.

calculations are therefore directly comparable to those from gas measurements at the same time. Estimates for March 20 are made on the assumption that the shape of the bubble distribution and rise velocities were identical on the two dates and only the magnitude alters with flow rate; thus we scale the March 13 results by $126.2/209$ to give the March 20 results. We also include in Table 1 for each day two “fits” of the parametric Eq. (16) to the gas measurements as described later.

There is a satisfactory agreement between gas-derived and bubble-derived values of the transfer velocity of methyl bromide for all cases. The theoretical relationship to the bubble distribution is expected to be almost wholly dependent on the flow rate, V_b , for this fairly soluble gas ($\alpha \approx 4$) and this is supported by the results here. Nitrous

oxide is a fairly soluble gas and is significantly affected by all the primary parameters. However, all fits that are compatible with the bubble measurements predict much higher bubble-mediated transfer for nitrous oxide than is retrieved from the gas measurements. It is possible that there is a systematic problem with nitrous oxide. The time series suggest that dissolved N_2O ceases to increase while far from equilibrium in the invasion experiments, which might suggest degradation of dissolved N_2O , however, no such process was detected (Rhee et al., submitted for publication) and the discrepancy between theory and experiment is unexplained.

The three least soluble gases, helium, sulphur hexafluoride and air produce the most intriguing results. Though they produce values of the correct order of

Table 2

Estimates of total and components (bubble-mediated and direct) of transfer velocity from analysis of gas measurements

	SF ₆	He	CH ₃ Br	N ₂ O
<i>March 13</i>				
K_T , total transfer velocity	58 (53–60.5)	70.5 (31–75.5)	13.25 (12.75–16.5)	12.5 (12.5–15.5)
K_b , bubble-mediated transfer velocity	46 (42–48)	58 (26–62)	2.75 (2.25–5)	3.5 (3.5–5.5)
K_d , direct transfer velocity	12 (11–12.5)	12.5 (5–13.5)	10.5 (10.5–11.5)	9 (9–10)
<i>March 20</i>				
K_T , total transfer velocity	42.5 (40–45)	74 (62–78.5)	8.5 (8.5–13.0)	15.5 (14–15.5)
K_b , bubble-mediated transfer velocity	36 (34–38)	60 (50–64)	2.0 (2–5.5)	5.5 (5.0–5.5)
K_d , direct transfer velocity	6.5 (6–7)	14 (12–14.5)	6.5 (6.5–7.5)	10 (9–10)

All values in cm/h. Best estimates are given followed by 90% confidence limits between brackets.

magnitude for each gas, no version of the individual bubble model produces satisfactory agreement with the gas-derived results. The basic problem is that the individual bubble model predicts much higher transfer velocities for He than for the other two gases (typically at a ratio of ≈ 2.5 between He and SF₆). A lower ratio is possible from the individual bubble model for very small and long-lived bubbles, but that clearly does not apply to the observed bubble distribution. Though there are significant uncertainties in the gas-derived results, they are not compatible with such a high ratio. The low ratio between values of bubble-mediated transfer velocity of helium and the other two gases might be explained by a significant effective void fraction and by the dense plume model. We explore that possibility next.

Reproducing something close to the gas-derived values requires both a much higher void fraction than is suggested by measurements of typical plumes ($\ll 1\%$) and higher individual bubble transfer velocities, j . Note that these j values are predicted from modelling and measurement of individual bubbles, usually rising in a quiescent liquid. It is plausible that values will be larger where turbulence from other bubbles affects each bubble. We look at modifications of the equations illustrated by Figs. 6 and 7 that can reproduce something closer to the gas-derived results reported in Table 1. The flow rate, Q_b , is well-established and therefore is fixed in all fits. Fit 1 is a modification of the result for the mixed clean and dirty bubbles; we preserve $n=0.6$ and $f=0.75$ from the fit in Fig. 6 but vary void fraction and the parameter, $\lambda (=Sc^{\eta}/(\chi\alpha))$. Similarly, Fit 2 is a modification for clean bubbles where $n=0.5$ and $f=0.9$ is retained from the fit shown in Fig. 7. Note that the variant described in Section 2.3 is used to predict the transfer velocity of air. We show contour plots of root mean error (averaged over the 5 gases) for various guesses of void fraction and λ in Figs. 11 and 12. Fig. 11 shows results for March 13. The minimum value of error is found for an unrealistically

high value of λ , and a very high void fraction ($\lambda=871$ and 14% for mixed clean and dirty, $\lambda=617$ and 13.7% for clean; both fits are included in Table 1). Fits based on lower, more realistic values of both parameters are much better than any of the zero void solutions, but no really satisfactory solution can be found. The difficulty in finding a close and sensible fit can be traced to the fact that the gas-derived value for He is very low and the value for air is very high, both of which are difficult to reproduce with a realistic model. This may result from higher errors in the experiment on March 13 as discussed in Section 4.2. Much more satisfactory fits are found for March 20 (Fig. 12 and Table 1). Both fits are wholly consistent with the gas-derived results (Tables 1 and 2) except for N₂O. The value of λ is higher in both cases than the standard value but in the case of clean bubbles (Fig. 12b; $\lambda=204$ compared to the standard $\lambda=175$) it is not greatly so. (In addition to limitations of the standard formulae already discussed, the revised parameter could be explained by a dominance of slightly smaller bubbles than has been assumed.) It is more difficult to understand how the implied void fraction (7.6% for the mixed case, 5.8% for the clean case) can be appropriate given the measured bubble plumes have a very low void fraction. However, the fit is very convincing and there is a strong implication that individual bubble transfer velocities, j , were higher than expected but the effect of this is counteracted by a strong suffocation effect. This underlines the difficulty in predicting gas transfer velocities from only bubble measurements and a few basic principles.

6. Summary of results and discussion

We first summarise the results from Sections 2 to 5.

- (1) Transfer velocity mediated by bubbles is generally dependent on both the solubility and the molecular diffusion coefficient of the gas in water.

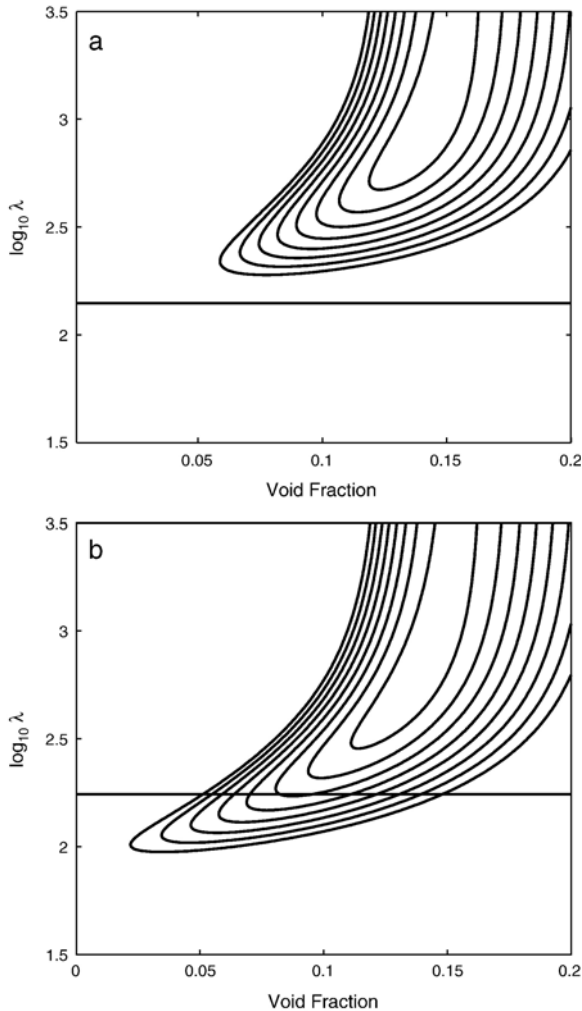


Fig. 11. Minimisation of misfit compared to gas-derived values of bubble-mediated transfer for March 13. (a) Based on “mixed” hydrodynamic parameters. (b) Based on “clean” hydrodynamic parameters. Contours of root mean square errors in intervals of 1 cm/h up to 20 cm/h; the innermost (lowest value) contour is at 13 cm/h. Horizontal lines are at the original estimates of λ .

- (2) In the limit of high solubility, transfer velocity is proportional to the volume flux of the bubbles, inversely proportional to solubility and independent of the diffusion coefficient.
- (3) In the limit of low solubility, sensitivity to solubility vanishes and for low void fractions, bubble-mediated transfer depends on the surface area of the bubbles and the diffusion coefficient (or Schmidt number) of a gas in a similar way to direct transfer.
- (4) If the void fraction of plumes is significant, bubble-mediated transfer is reduced, especially for gases of low solubility and high diffusion coefficient.

- (5) Bubble-mediated gas transfer velocities were calculated from measured bubble distributions and also estimated from gas measurements, though both estimates are imprecise.
- (6) The theoretical transfer from the measured bubble distribution can be fitted by a simple parametric equation based on Results (2) to (4) above.
- (7) Estimates of bubble-mediated transfer velocity from gas measurements are broadly in line with calculations from the bubble distribution, but there are significant discrepancies.
- (8) The bubble-mediated transfer velocities estimated from helium, air and sulphur hexafluoride

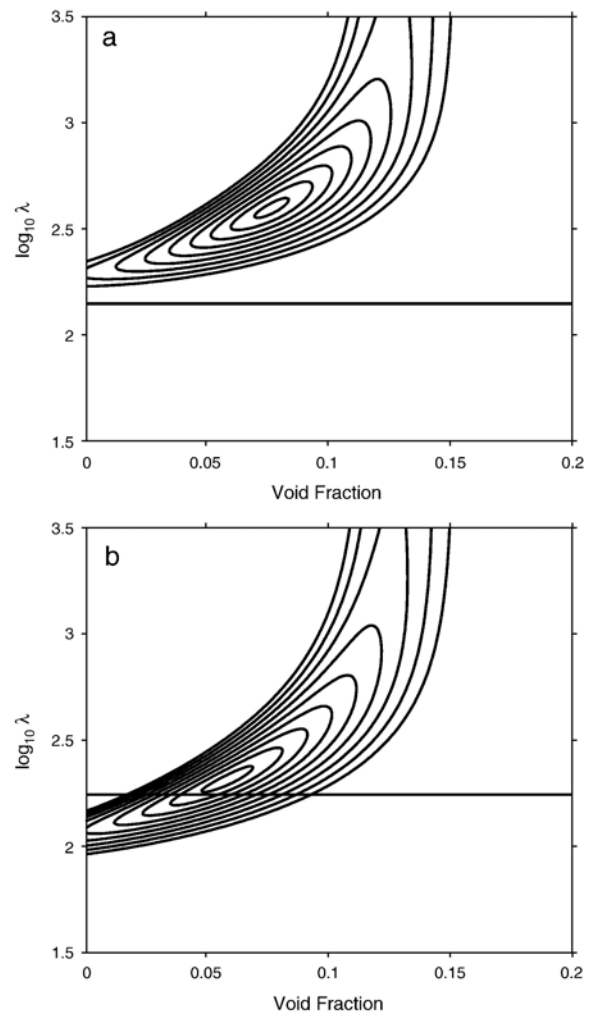


Fig. 12. Minimisation of misfit compared to gas-derived values of bubble-mediated transfer for March 20. (a) Based on “mixed” hydrodynamic parameters. (b) Based on “clean” hydrodynamic parameters. Contours of root mean square errors in intervals of 1 cm/h up to 10 cm/h; the innermost (lowest value) contour is at 2 cm/h. Horizontal lines are at the original estimates of λ .

measurements are large and similar in value. This insensitivity among insoluble gases can best be explained by the effect of a finite void fraction.

Experiments have been conducted in fresh water with an artificial source of bubbles. The most significant effect of water type is on bubble distribution and since this distribution is inevitably unrealistic with the artificial source, the water type is not significant. The range of bubble size and the time to surface is broadly similar to those bubbles expected to dominate air–sea gas transfer (Woolf, 1993), so that while the experiments were not close simulations of natural processes, they are a useful test of the models.

We have successfully separated the contributions of “direct” transfer (directly across the wavy water surface) and “bubble-mediated” transfer (*via* exchange across the surface of bubbles). The direct transfer is associated with a number of mechanisms including the action of wind and waves *and* the disruption by the surfacing bubbles. The influence of surfacing bubbles can be estimated in principle by comparing the estimated direct exchange in the experiments described above with experiments in similar wind and wave conditions but without aeration. However, though the direct transfer is generally greater in the experiments with aeration, there is not a clear enhancement. It seems that the transfer velocity associated with the surfacing bubbles was < 10 cm/h, but is uncertain. Note also, that the complete effect of turbulence associated with breaking waves is not simulated in these experiments and the total effect may be more substantial (Asher et al., 1996).

The bubble-mediated transfer is very high for some gases. The factors influencing bubble-mediated transfer were reviewed by Woolf (1997), and have been extended in this study (particularly to the case of high-void-fraction plumes). Previous attempts to match measured bubble distributions to measured transfer velocities have met considerable difficulties, mainly due to difficulty in measuring near-surface bubble populations (Leifer et al., 1995). Our new experimental results give some confidence that useful predictions of bubble-mediated transfer can be made from measurements of bubble distributions if these are adequate. However, these predictions depend on detailed bubble distributions including void fractions and even then are unlikely to be precise. Our results suggest that the effective void fraction may be high even in apparently diffuse bubble plumes. A special characteristic of the simulation may be responsible, which is that each bubble from an aerator tends to follow in the wake of a preceding bubble. Formulae for clean bubbles also appear to explain the results better, this may be a combination of the fact that the bubbles are not particularly small and as a result of the pro-

longed operation of the aerators, which will effectively strip most surface-active material from the water column (slick material will tend to accumulate near the “beach” of the tank away from the aerators).

Results indicate a complicated relationship between the transfer velocity of different insoluble gases (e.g. helium, sulphur hexafluoride and air) and between these gases and more soluble gases of greater geophysical significance (e.g. nitrous oxide and carbon dioxide). This is significant given that these highly insoluble gases are the basis of some of the most important field estimates of transfer velocity. For the case of the dual-tracer method (helium and sulphur hexafluoride) Asher and Wanninkhof (1998) have estimated necessary corrections from the results of a laboratory simulation (Asher et al., 1996). These corrections suggest that the uncorrected dual-tracer method will generally overestimate the transfer velocity of carbon dioxide (Asher and Wanninkhof, 1998). Both theory and experiments described here illustrate that the relative value of transfer velocities for different gases is highly sensitive to void fraction and bubble distribution, so that it is uncertain if a single set of corrections will be adequate for all cases. Where the void fraction is very high the transfer velocity of helium and sulphur hexafluoride will be almost equal, and thus the resulting transfer will be “invisible” to the traditional dual-tracer method. Thus if very high void fraction bubble plumes dominate, it is possible that the uncorrected dual-tracer method may underestimate the transfer velocity of carbon dioxide. Measurements of the near-surface bubble plumes during dual-tracer experiments may be required for full interpretation of the dual tracer results.

Notation

Subscripts

g	Generic gaseous reservoir
a	Main gas reservoir (headspace of tank)
atm	Atmospheric (outside laboratory)
b	Bubble or bubble-mediated
l	Generic liquid reservoir
w	Main liquid reservoir (water in tank)
i	Interstitial water
p	Plume water
T	Total
d	Direct
o	Original
f	Final

Main symbols

A	Surface area; A_d is the surface area of the tank
C	Concentration

D	Molecular diffusion constant
g	Acceleration due to gravity
j	Individual bubble gas transfer velocity
K	Transfer velocity
K_A	Transfer velocity integrated over interfacial area
Q	Volume flux (per unit time, unit interfacial area)
r	Radius
Sc	Schmidt number
t	Time
V	Volume
z	Depth
α	Ostwald solubility
Δ	Equilibrium supersaturation resulting from direct and bubble-mediated transfer
δ	Equilibrium supersaturation resulting from bubble-mediated transfer
γ	Surface tension
ρ	Density
Σ	Net source of gas
τ	Time constant

Acknowledgements

Primary support for the experiments was provided by the European Commission EC DG XII in connection with the LUMINY project (ENV4-CT95-0080). The support of all staff at IRPHE is also gratefully acknowledged. The completion of this research was supported by the United Kingdom Natural Environment Research Council (NERC) through the Centre for observation of Air–Sea Interactions and fluxes (CASIX). This is CASIX Publication No. 37. UK participants were also supported by the Natural Environment Research Council through Core Programmes at NOC and PML.

References

- Asher, W.E., Wanninkhof, R., 1998. The effect of bubble-mediated gas transfer on purposeful dual-gaseous tracer experiments. *J. Geophys. Res.* 103, 10555–10560.
- Asher, W.E., Karle, L.M., Higgins, B.J., Farley, P.J., Monahan, E.C., Leifer, I.S., 1996. The influence of bubble plumes on air–water gas transfer velocities. *J. Geophys. Res.* 101, 12027–12041.
- Bowyer, P., Woolf, D.K., 2004. Gas exchange and bubble-induced supersaturation in a wind-wave tank. *J. Atmos. Ocean. Technol.* 21 (12), 1925–1935.
- Cirpka, O., Reichert, P., Wanner, O., Müller, S.R., Schwarzenbach, R.P., 1993. Gas exchange at river cascades: field experiments and model calculations. *Environ. Sci. Technol.* 27, 2086–2097.
- De Leeuw, G., Kunz, G.J., Caulliez, G., Woolf, D.K., Bowyer, P., Leifer, I., Nightingale, P., Liddicoat, M., Rhee, T.S., Andreae, M.O., Larsen, S.E., Hansen, F.A., Lund, S., 2002. LUMINY: an overview. In: Donelan, M.A., Drennan, W.M., Salzman, E.S., Wanninkhof, R. (Eds.), *Gas Transfer at Water Surfaces*, Geophysical Monograph, vol. 127. AGU, Washington, pp. 291–294.
- Keeling, R.F., 1993. On the role of large bubbles in air–sea gas exchange and supersaturation in the ocean. *J. Mar. Res.* 51, 237–271.
- Kitaigorodskii, S., 1984. On the fluid dynamical theory of turbulent gas transfer across an air–sea interface in the presence of breaking wind waves. *J. Phys. Oceanogr.* 14, 960–972.
- Krysell, M., Nightingale, P.D., 1994. Low molecular weight halocarbons in the Humber and Rhine estuaries determined using a new purge and trap gas chromatographic technique. *Cont. Shelf Res.* 14, 1311–1329.
- Law, C.S., Watson, A.J., Liddicoat, M.I., 1994. Automated vacuum analysis of sulphur hexafluoride in sea water: derivation of the atmospheric trend (1970–1993) and potential as transient tracer. *Mar. Chem.* 48, 57–69.
- Leifer, I., de Leeuw, G., 2006. Bubbles generated from wind-steepened breaking waves: Part 1. Bubble from bubble plumes. *J. Geophys. Res.* 111, C06020. doi:10.1029/2004JC002673.
- Leifer, I., Patro, R.K., 2002. The bubble mechanism for methane transport from the shallow sea bed to the sea surface: a review and sensitivity study. *Cont. Shelf Res.* 22, 2409–2428.
- Leifer, I.S., Asher, W.E., Farley, P.J., 1995. A validation study of bubble mediated air–sea gas transfer modeling for trace gases. In: Jähne, B., Monahan, E.C. (Eds.), *Air–Water Gas Transfer*. AEON Verlag, Heidelberg, pp. 269–283.
- Leifer, I., de Leeuw, G., Cohen, L.H., 2000. Secondary bubble production from breaking waves: the bubble burst mechanism. *Geophys. Res. Lett.* 27, 4077–4080.
- Leifer, I., de Leeuw, G., Cohen, L.H., 2003. Optical measurement of bubbles: system design and application. *J. Atmos. Ocean. Technol.* 20, 1317–1332.
- Leifer, I., Caulliez, G., de Leeuw, G., 2006. Bubbles generated from wind-steepened breaking waves: Part 2. Bubble plumes, bubbles, and wave characteristics. *J. Geophys. Res.* 111, C06021. doi:10.1029/2004JC002676.
- Liss, P.S., Merlivat, L., 1986. Air–sea gas exchange rates: introduction and synthesis. In: Buat-Menard, P. (Ed.), *The Role of Air–Sea Exchange in Geochemical Cycling*. Reidel, Washington, pp. 113–129.
- Memery, L., Merlivat, L., 1985. Modelling of gas flux through bubbles at an air–water interface. *Tellus* 37B, 272–285.
- Merlivat, L., Memery, L., 1983. Gas exchange across an air–water interface: experimental results and modelling of bubble contribution to transfer. *J. Geophys. Res.* 88, 707–724.
- Monahan, E.C., Spillane, M.C., 1984. The role of oceanic whitecaps in air–sea gas exchange. In: Brutsaert, W., Jirka, G.H. (Eds.), *Gas Transfer at Water Surfaces*. Kluwer Academic Publisher, Dordrecht, pp. 495–503.
- Nightingale, P.D., Malin, G., Law, C.S., Watson, A.J., Liss, P.S., Liddicoat, M.I., Boutin, J., Upstill-Goddard, R.C., 2000. In situ evaluation of air–sea gas exchange parameterizations using novel conservative and volatile tracers. *Glob. Biogeochem. Cycles* 14, 373–387.
- Patro, R., Leifer, I., Bowyer, P., 2002. Better bubble process modeling: improved bubble hydrodynamics parameterization. In: Donelan, M.A., Drennan, W.M., Salzman, E.S., Wanninkhof, R. (Eds.), *Gas Transfer at Water Surfaces*. Geophysical Monograph, vol. 127. AGU, Washington, pp. 315–320.
- Press, W.H., Teukolsky, S.A., Vetterling, W.T., Flannery, B.P., 1992. *Numerical Recipes in C*. Cambridge University Press, Cambridge, UK. 994 pp.
- Rhee, T.S., Nightingale, P.D., Woolf, D.K., Caulliez, G., Bowyer, P., Andreae, M.O., submitted for publication. Suppression of gas transfer by regular waves observed in a large wind-wave tunnel facility. *J. Geophys. Res.*

- Upstill-Goddard, R.C., Watson, A.J., Wood, J., Liddicoat, M.I., 1991. Sulphur hexafluoride and helium-3 as sea-water tracers: deployment techniques and continuous underway analysis for sulphur hexafluoride. *Anal. Chim. Acta* 249, 555–562.
- Wanninkhof, R., 1992. Relationship between gas exchange and wind speed over the ocean. *J. Geophys. Res.* 97, 7373–7381.
- Wanninkhof, R., McGillis, W.R., 1999. A cubic relationship between air–sea CO₂ exchange and wind speed. *Geophys. Res. Lett.* 26, 1889–1892.
- Weiss, R.F., Woz, F.A.V., Salameh, P.K., 1992. Surface Water and Atmospheric Carbon Dioxide and Nitrous Oxide Observations by Shipboard Automated Gas Chromatography: Results from Expeditions between 1977 and 1990. Oak Ridge National Laboratory, Oak Ridge, Tennessee.
- Woolf, D.K., 1993. Bubbles and the air–sea transfer velocity of gases. *Atmos.-Ocean* 31 (4), 517–540.
- Woolf, D.K., 1995. Energy dissipation through wave breaking and the air–sea exchange of gases. In: Jähne, B., Monahan, E.C. (Eds.), *Air–Water Gas Transfer*. AEON Verlag, Heidelberg, pp. 185–195.
- Woolf, D.K., 1997. Bubbles and their role in air–sea gas exchange. In: Liss, P.S., Duce, R.A. (Eds.), *The Sea Surface and Global Change*. Cambridge University Press, pp. 173–205.
- Woolf, D.K., 2005. Parametrization of gas transfer velocities and sea-state-dependent wave breaking. *Tellus* 57B, 87–94.
- Woolf, D.K., Thorpe, S.A., 1991. Bubbles and the air–sea exchange of gases in near-saturation conditions. *J. Mar. Res.* 49, 435–466.